

Portland State University

**PDXScholar**

---

Geography Faculty Publications and  
Presentations

Geography

---

6-7-2022

# Regional and Elevational Patterns of Extreme Heat Stress Change in the US

Colin Raymond

*Jet Propulsion Laboratory, California Institute of Technology*

Duane E. Waliser

*NASA Jet Propulsion Laboratory*

Bin Guan

*California Institute of Technology*

Huikyo Lee

*Jet Propulsion Laboratory, California Institute of Technology*

Paul Loikith

*Portland State University, ploikith@pdx.edu*

*See next page for additional authors*

Follow this and additional works at: [https://pdxscholar.library.pdx.edu/geog\\_fac](https://pdxscholar.library.pdx.edu/geog_fac)



Part of the [Geography Commons](#)

**Let us know how access to this document benefits you.**

---

## Citation Details

Raymond, C., Waliser, D., Guan, B., Lee, H., Loikith, P., Massoud, E., ... & Wootten, A. (2022). Regional and elevational patterns of extreme heat stress change in the US. *Environmental Research Letters*.

This Article is brought to you for free and open access. It has been accepted for inclusion in Geography Faculty Publications and Presentations by an authorized administrator of PDXScholar. Please contact us if we can make this document more accessible: [pdxscholar@pdx.edu](mailto:pdxscholar@pdx.edu).

---

**Authors**

Colin Raymond, Duane E. Waliser, Bin Guan, Huikyo Lee, Paul Loikith, Elias C. Massoud, Agniv Sengupta, Deepthi Singh, and Adrienne Wootten

LETTER • **OPEN ACCESS**

## Regional and elevational patterns of extreme heat stress change in the US

To cite this article: Colin Raymond *et al* 2022 *Environ. Res. Lett.* **17** 064046

View the [article online](#) for updates and enhancements.

You may also like

- [Aerosol-modulated heat stress in the present and future climate of India](#)  
Sagnik Dey, Rohit Kumar Choudhary, Abhishek Upadhyay et al.
- [Irrigation offsets wheat yield reductions from warming temperatures](#)  
Jesse Tack, Andrew Barkley and Nathan Hendricks
- [Estimating heat stress from climate-based indicators: present-day biases and future spreads in the CMIP5 global climate model ensemble](#)  
Y Zhao, A Ducharme, B Sultan et al.



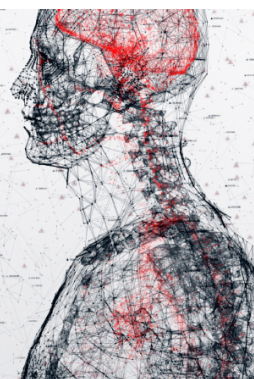
physicsworld

AI in medical physics week

20–24 June 2022

Join live presentations from leading experts  
in the field of AI in medical physics.

[physicsworld.com/medical-physics](https://physicsworld.com/medical-physics)



ENVIRONMENTAL RESEARCH  
LETTERS

## LETTER

Regional and elevational patterns of extreme heat stress change  
in the US

## OPEN ACCESS

RECEIVED  
24 August 2021REVISED  
9 May 2022ACCEPTED FOR PUBLICATION  
25 May 2022PUBLISHED  
7 June 2022

Original content from  
this work may be used  
under the terms of the  
[Creative Commons  
Attribution 4.0 licence](#).

Any further distribution  
of this work must  
maintain attribution to  
the author(s) and the title  
of the work, journal  
citation and DOI.



Colin Raymond<sup>1,\*</sup> , Duane Waliser<sup>1</sup>, Bin Guan<sup>1,2</sup>, Huikyo Lee<sup>1</sup>, Paul Loikith<sup>3</sup> , Elias Massoud<sup>4</sup>,  
Agniv Sengupta<sup>4,5</sup> , Deepti Singh<sup>6</sup> and Adrienne Wootten<sup>7</sup>

<sup>1</sup> Jet Propulsion Laboratory/California Institute of Technology, Pasadena, CA, United States of America

<sup>2</sup> Joint Institute for Regional Earth System Science and Engineering, University of California, Los Angeles, Los Angeles, CA,  
United States of America

<sup>3</sup> Portland State University, Portland, OR, United States of America

<sup>4</sup> University of California, Berkeley, Berkeley, CA, United States of America

<sup>5</sup> University of California, San Diego, San Diego, CA, United States of America

<sup>6</sup> Washington State University, Vancouver, WA, United States of America

<sup>7</sup> South Central Climate Science Center, University of Oklahoma, Norman, OK, United States of America

\* Author to whom any correspondence should be addressed.

E-mail: [colin.raymond@jpl.nasa.gov](mailto:colin.raymond@jpl.nasa.gov)

**Keywords:** heat stress, humidity, elevation, projections

Supplementary material for this article is available [online](#)

**Abstract**

Increasing severity of extreme heat is a hallmark of climate change. Its impacts depend on temperature but also on moisture and solar radiation, each with distinct spatial patterns and vertical profiles. Here, we consider these variables' combined effect on extreme heat stress, as measured by the environmental stress index, using a suite of high-resolution climate simulations for historical (1980–2005) and future (2074–2099, Representative Concentration Pathway 8.5 (RCP8.5)) periods. We find that observed extreme heat stress drops off nearly linearly with elevation above a coastal zone, at a rate that is larger in more humid regions. Future projections indicate dramatic relative increases whereby the historical top 1% summer heat stress value may occur on about 25%–50% of future summer days under the RCP8.5 scenario. Heat stress increases tend to be larger at higher latitudes and in areas of greater temperature increase, although in the southern and eastern US moisture increases are nearly as important. Imprinted on top of this dominant pattern we find secondary effects of smaller heat stress increases near ocean coastlines, notably along the Pacific coast, and larger increases in mountains, notably the Sierra Nevada and southern Appalachians. This differential warming is attributable to the greater warming of land relative to ocean, and to larger temperature increases at higher elevations outweighing larger water-vapor increases at lower elevations. All together, our results aid in furthering knowledge about drivers and characteristics that shape future extreme heat stress at scales difficult to capture in global assessments.

**1. Introduction**

Large increases in extreme temperature are a robust feature of climate-change projections (Li *et al* 2021). Furthermore, in most of the United States, there is a greater expected rise in heat waves when considering moisture and temperature together than temperature alone (Barnston *et al* 2020). This translates to a growing risk of extreme heat stress (Coffel *et al* 2018, Li *et al* 2020)—the combination of temperature and other climate variables, like humidity,

known to negatively affect the human body's functioning in hot weather—with major implications for human health (Hanna and Tait 2015, Kjellstrom *et al* 2016, Mora *et al* 2017). The effect of high temperatures on water and energy supply and demand, ecosystems, and economic and agricultural output can also be relatively larger or smaller according to the co-occurring humidity (Dunne *et al* 2013, Harpold and Brooks 2018, Haqiqi *et al* 2021). Even regions with comparatively mild climates can be strongly affected by heat stress due to a lack of physiological,

behavioral, or infrastructural preparedness, stemming from resource limitations or perceived lack of need for investments such as air conditioning or heat-resistant materials (Ferranti *et al* 2016, Guirguis *et al* 2018). As a result of this conditioning on the historical range, heat stress's impacts (e.g. as measured by wet-bulb globe temperature) tend to increase exponentially in response to small changes near or beyond the high end of its historical values (Wu *et al* 2014, Cheng *et al* 2019).

While recent studies have considered projections of extreme heat (Broadbent *et al* 2020) or heat stress (Barnston *et al* 2020, Chen *et al* 2020, Li *et al* 2020), none have included a focus on how these increases may vary by elevation. This knowledge gap exists despite greater warming at higher elevations having been shown in observations and projections for mountain ranges including the Cascades, Sierra Nevada, Rockies, Alps, and Himalayas (Rangwala *et al* 2012, 2013, Pepin *et al* 2015, Rupp *et al* 2017, Minder *et al* 2018, Palazzi *et al* 2018).

Although elevation-dependent warming is relatively smaller in summer than in other seasons, it is significant: by the late 21st century, Western-US daily-maximum summer temperatures are expected to increase by approximately an additional 0.5 °C with each 1000 m of elevation gain, driven by a shift toward drier atmospheric and land-surface conditions and less cloud cover at higher elevations; little to no such effect is seen for daily minimum temperatures (Rangwala *et al* 2012, Palazzi *et al* 2018). Regional analyses have revealed the importance of additional factors, such as smaller future temperature changes over oceans affecting nearby coasts and thus creating an elevational signature (Raymond and Mankin 2019). For example, in the Northwest, projected soil drying leads to summer-mean temperatures increasing most around 1500 m, with this increase being less toward sea level (due to persistent marine cooling) and toward higher elevations (due to smaller decreases in soil moisture) (Rupp *et al* 2017). In the Southwest, the differential temperature increase proceeds fairly linearly from low to high elevations (Rupp *et al* 2017). Due to the drop-off in specific humidity with elevation, heat stress at higher elevations is more closely connected with heat than moisture, leaving open the possibility that heat stress could also have a positive elevation dependence. Conclusive analyses for elevation dependence of any kind have often been limited by the 5–30 km grid spacing of regional climate models and the sparseness of observational data in mountainous areas.

In the western US—where population centers and important transportation, water, and power infrastructure are situated at elevations ranging from sea level to above 2000 m—understanding current and future elevation profiles of extreme heat stress would aid in assessing the competing effects of projected large extreme-temperature increases (Barnston *et al*

2020): circulation and vegetation changes lead to strong drying and heightened wildfire risk (Mankin *et al* 2017, Brown *et al* 2021), but a weaker North American Monsoon and stronger evapotranspiration lead to increases in water vapor (Pascale *et al* 2017). In the eastern US, elevation variability is smaller than in the West but absolute humidities and thus baseline heat stress values are higher, creating the potential for notable divergence from regional means in mountain and coastal communities.

Here, we focus on evaluating climatically extreme (99th percentile) heat stress over the US and its future changes under Representative Concentration Pathway 8.5 (RCP8.5) due to three variables: 2 m temperature ( $T$ ), 2 m water vapor content ( $q$ ), and surface downwelling solar radiation ( $r$ ) (Steadman 1979, Moran *et al* 2001). Elevation dependence in historical values of each variable and in the processes influencing them under climate change leads to uncertainty about their combined effect on extreme heat stress. For example, elevation-dependent warming and enhanced summer drying at higher elevations would cause offsetting effects on heat stress; solar radiation represents an additional factor which affects the rate of heat transfer from the human body (Kjellstrom *et al* 2016) and is itself affected by vertical profiles of atmospheric thickness and optical depth (Annear and Wells 2007). Motivated by a desire to build physical understanding and lay the groundwork for assessing potential impacts of heat stress on human health and ecosystems, the aim of our study is to determine how temperature, moisture, and radiation interact to shape extreme heat stress under climate change across regions and elevations of the US.

## 2. Data and methods

We compare equal-length subsets of the historical (1980–2005) and RCP8.5 (2074–2099) simulations for 20 models from the Coupled Model Intercomparison Project 5 (CMIP5) that have been statistically downscaled and optimized via the Multivariate Adaptive Constructed Analogs (MACA) method to match an observational reference, the gridMET reanalysis (Abatzoglou and Brown 2012, Abatzoglou 2013). This correction is necessary because of model biases in representing historical climates, and while it results in improvements (Abatzoglou and Brown 2012), it does not address process errors, meaning that considerable model-related uncertainty remains (Lorenz *et al* 2018). The resultant MACA-based dataset is available at daily, ~4 km resolution, and is a preferred choice for representing regional and sub-regional extreme events, including in high-elevation and coastal areas (e.g. Jiang *et al* 2018).

To represent extreme heat stress, we use the environmental stress index (ESI) (Moran *et al* 2001, 2003), which combines daily-maximum temperature ( $T$ ),

daily-mean specific humidity ( $q$ ) (converted to relative humidity [RH]), and daily-mean shortwave radiation ( $r$ ):

$$\text{ESI} = 0.63T - 0.03\text{RH} + 0.002r + 0.0054(T * \text{RH}) - 0.073(0.1 + r)^{-1}$$

for ESI in °C, with temperature  $T$  in °C, shortwave radiation  $r$  in  $\text{W m}^{-2}$ , and RH in %.

The timescales of the variables follows Coffel *et al* (2018), who argue that daily-maximum  $T$  and daily-mean  $q$  together approximate daily-maximum heat stress. As a supplementary analysis we also compute ESI using daily-minimum  $T$  and daily-mean  $q$ , reflecting the additional value this version of the metric may have for heat-stress impacts.

The ESI correlates highly ( $r \sim 0.99$ ) with the heat-stress-relevant but more-difficult-to-calculate wet-bulb globe temperature (Moran *et al* 2001), while including solar-radiation effects that are absent in wet-bulb temperature and other common heat indices and that are essential to a complete understanding of heat stress (Hanna and Tait 2015, Kjellstrom *et al* 2016, Gao *et al* 2017). It also has nearly the same values as wet-bulb globe temperature, whose impacts rise rapidly above 28 °C and especially above 32 °C (Moran *et al* 2001, Cheng *et al* 2019). The variables that constitute ESI, therefore, serve as a good approximation of potential impacts to human health, productivity, and energy demand (Kjellstrom *et al* 2016). However, actual heat-related impacts vary considerably according to population demographics, acclimation, socioeconomic status, physical activity, clothing, and other factors (meaning that the same impacts can occur at lower levels of heat stress depending on population vulnerability); this makes the health relevance of any particular heat threshold only approximate (Kjellstrom *et al* 2016, Cheng *et al* 2019, Vicedo-Cabrera *et al* 2021).

We find that, in the historical period, the MACA dataset exhibits biases relative to gridMET that are generally less than 1.5 °C for extreme  $T$  and 0.5  $\text{g kg}^{-1}$  for extreme  $q$ ; these correspond to approximately 0.75 and 0.5 when normalized against the distribution of the 99th percentile (figures S1 and S2 (available online at [stacks.iop.org/ERL/17/064046/mmedia](https://stacks.iop.org/ERL/17/064046/mmedia))). Regional and global models have previously struggled to replicate the elevation dependence of observed trends in summer extreme  $T$  (Pepin *et al* 2015), but we find that the MACA dataset is typically at least as consistent with two observational datasets—the ERA5 reanalysis and the global weather stations of the Hadley Centre Integrated Surface Database (HadISD)—as they are with each other (figure S3) (Dunn *et al* 2012, Hersbach *et al* 2020).

Consistent with our focus on extreme events, we compute the 99th percentile of daily ESI for each model over the extended summer season (May–September, MJJAS), averaged over 1980–2005 and

separately 2074–2099. The selection of the 99th percentile follows previous studies (Chen *et al* 2020, Vicedo-Cabrera *et al* 2021), but we do not intend to comprehensively characterize drivers of heat-stress risk; a more epidemiologically oriented study might consider multiple percentiles, or both daytime and nighttime values. For both ESI and its constituent variables, we take the mean of models within the central two quartiles of the distribution, as a balance between representing the model spread and ensuring spatial consistency. We term this quantity the ‘extreme ESI’ for a time period. Model versions produced by the same modeling center, or whose outputs are highly correlated, have weights reduced such that their sum equals that of a single more-independent model (table S1; Knutti *et al* 2013). We consider extreme ESI for individual gridpoints and as a mean value over the seven National Climate Assessment regions of the contiguous US (USGCRP 2017): Northwest (NW), Southwest (SW), Northern Great Plains (NGP), Southern Great Plains (SGP), Midwest (MW), Southeast (SE), and Northeast (NE) (figure 1(a)). Results are computed for elevation bins in 50 m increments, with regional means computed in all cases where there are at least 25 gridpoints in a bin. While we use only data from the RCP8.5 scenario, to ease inter-scenario comparisons we include supplemental figures showing changes per degree of change in global-mean surface air temperature (figures S4 and S5; Collins *et al* 2013).

### 3. Results and discussion

Historical extreme ESI values are highest in the SW deserts, SGP, MW, and SE, consistent with previous work connecting heat stress most closely to extreme  $q$  (figure 1(b)) (Raymond *et al* 2017). Lower values are apparent in the mountains of both the western and eastern US, as is a general latitudinal gradient. Projected extreme heat stress increases are larger at higher latitudes and in interior areas of the western US (figure 1(c)), broadly matching patterns for extreme  $T$  (Wuebbles *et al* 2015, Vose *et al* 2017, Raymond and Mankin 2019). Coastal areas including California, the Gulf Coast, and Florida experience smaller increases. The influence of elevation on projected changes is moderate and can be seen most clearly in the Great Basin area of the SW.

The projected increases in extreme ESI are more dramatic when the future climate is compared against the historical 99th percentile (figure 1(d)): this threshold is expected to be exceeded on 15% to 60% of future summer days, with a spatial pattern largely controlled by historical variability but also bearing some elevational signature, such as in the central Sierra Nevada and southern Appalachian Mountains. This result adds new detail to previous global-scale studies (Dosio *et al* 2018), and in the regional means

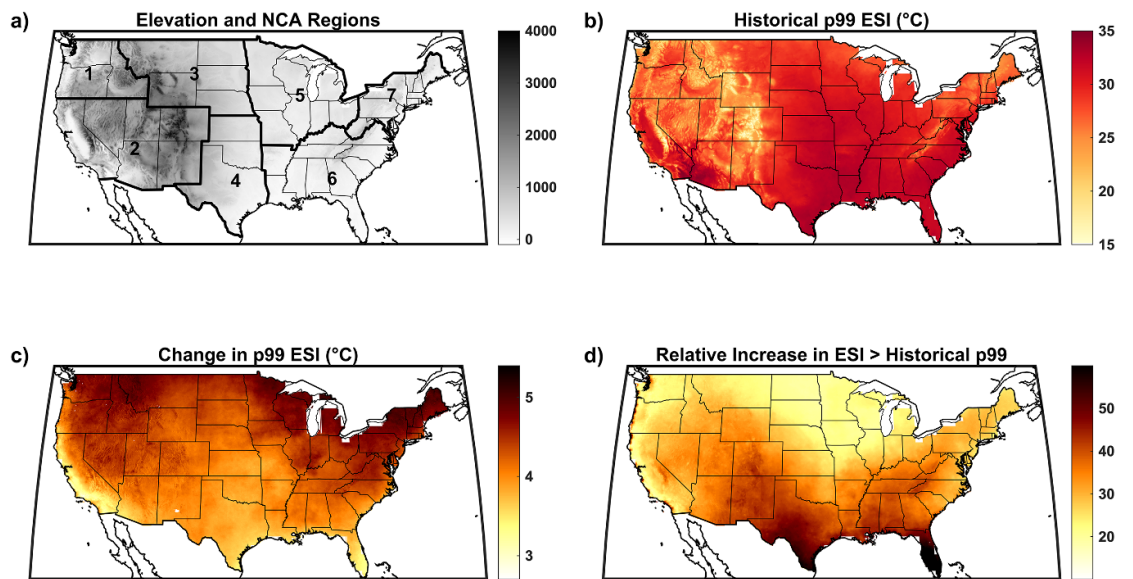


**Figure 1.** (a) Elevation as represented in the Multivariate Adaptive Constructed Analogs downscaled dataset. Regions are 1: Northwest; 2: Southwest; 3: Northern Great Plains; 4: Southern Great Plains; 5: Midwest; 6: Southeast; 7: Northeast. (b) 99th-percentile environmental stress index (ESI) (°C) for May–September, 1980–2005. (c) Change in 99th-percentile ESI from 1980–2005 to 2074–2099. (d) Factor by which May–September days above the ESI historical 99th percentile increase in frequency between 1980–2005 and 2074–2099 (50 = 50 times more often).

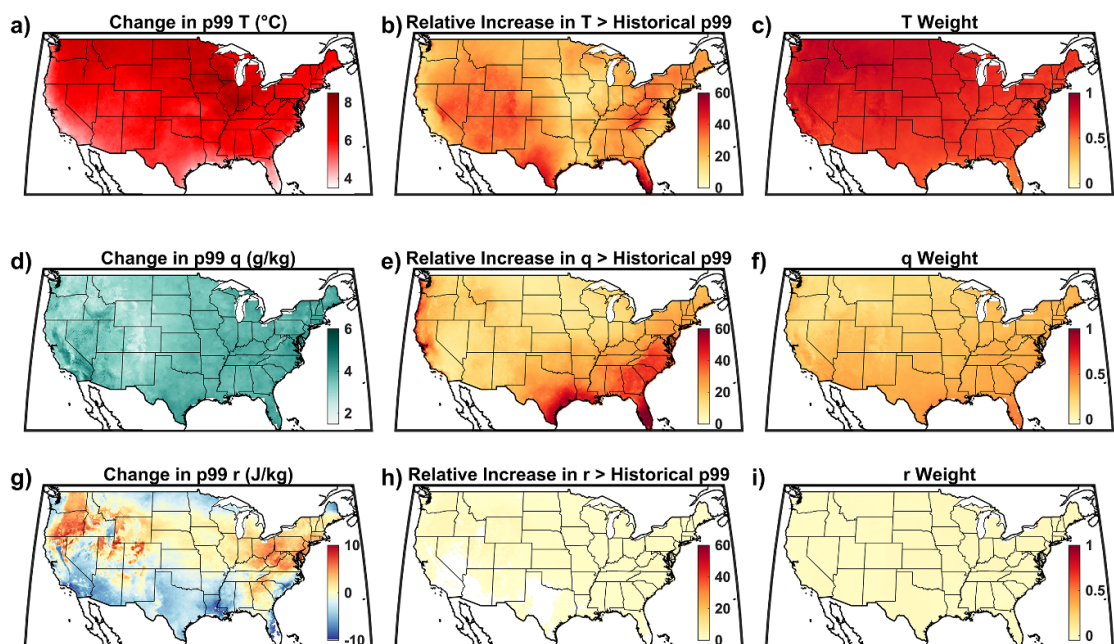


**Figure 2.** (a) Projected change in the 99th percentile of May–September temperature  $T$  from 1980–2005 to 2074–2099. (d), (g) As in (a) but for specific humidity  $q$  and shortwave radiation  $r$ . (b) Factor by which May–September days above the  $T$  historical 99th percentile increase in frequency between 1980–2005 and 2074–2099 (50 = 50 times more often). (e), (h) As in (b) but for  $q$  and  $r$ . (c) Proportion of extreme-environmental-stress-index change attributable to  $T$ , determined by using projected future  $T$  and historical  $q$  and  $r$ . (f), (i) As in (c) but for change attributable to  $q$  and  $r$ .

is consistent with findings from dynamically downscaled simulations (Zobel *et al* 2017).

We decompose the overall pattern of ESI changes shown in figure 1 by considering the contributions from changes in each variable (figure 2).  $T$  increases account for 60%–90% of the ESI increase, a proportion which is largest in the NW; the proportion

attributable to  $q$  increases ranges from less than 10% in parts of the West to more than 40% in the SE; and the  $r$  proportion is less than 5% everywhere (figures 2(c), (f) and (i)). We find the largest changes in extreme  $T$ , of up to 8 °C, in the MW, NGP, and NW, while coastal areas of California, Texas, and Florida see changes of only around 4 °C, in

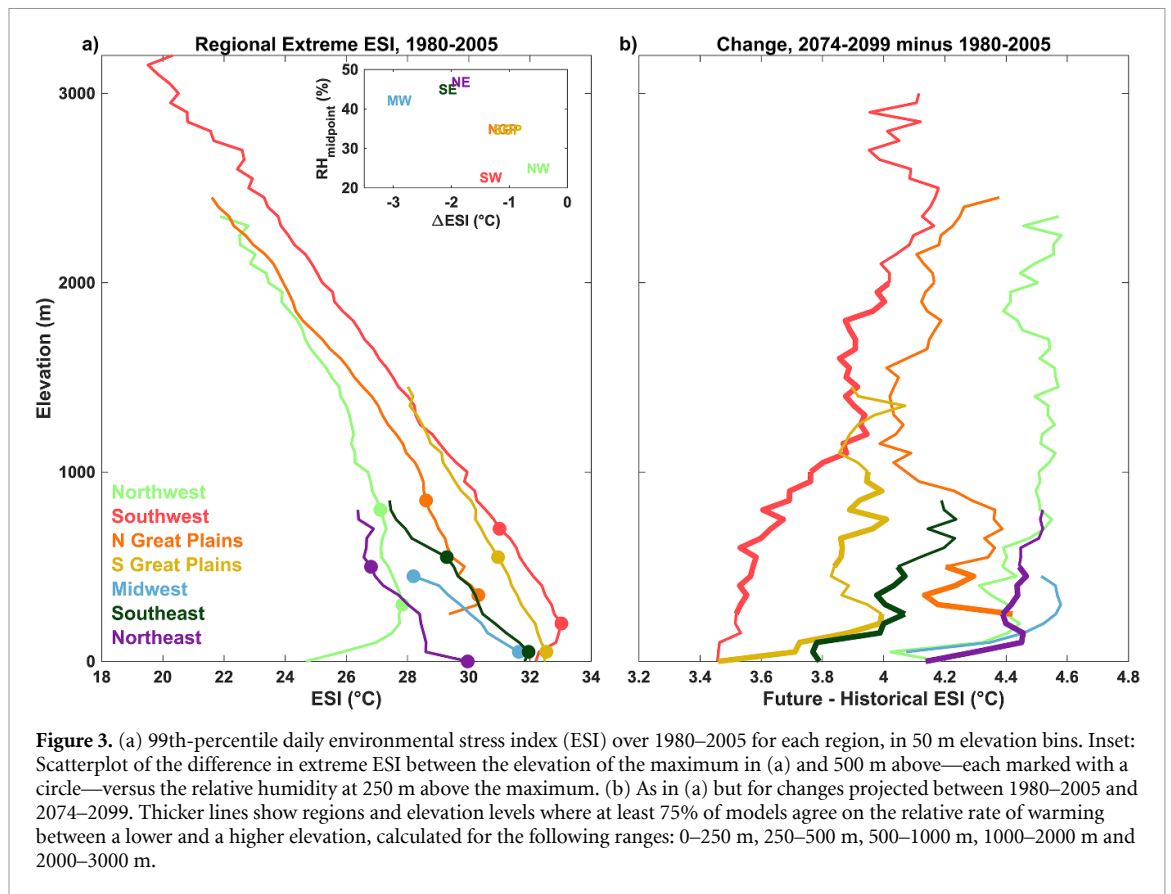


**Figure 3.** (a) 99th-percentile daily environmental stress index (ESI) over 1980–2005 for each region, in 50 m elevation bins. Inset: Scatterplot of the difference in extreme ESI between the elevation of the maximum in (a) and 500 m above—each marked with a circle—versus the relative humidity at 250 m above the maximum. (b) As in (a) but for changes projected between 1980–2005 and 2074–2099. Thicker lines show regions and elevation levels where at least 75% of models agree on the relative rate of warming between a lower and a higher elevation, calculated for the following ranges: 0–250 m, 250–500 m, 500–1000 m, 1000–2000 m and 2000–3000 m.

agreement with prior results (figure 2(a)) (Wuebbles *et al* 2015). However, the latter regions experience the largest relative increases, due to their smaller historical variability. Few, if any, topographic effects are seen. In contrast, extreme  $q$  (figure 2(d)) increases sharply in the eastern US but also in elevation-specific portions of the West that are comparatively drier than the East, such as the California Central Valley and Idaho’s Snake River Plain. Extreme radiation has positive changes in the greater Appalachians, northern Rockies, and interior NW, and negative changes in Florida, the Gulf Coast, and southern California (figure 2(f)); in the former regions, model output may reflect connected biases in temperature, cloudiness, and land-atmosphere coupling (Cheruy *et al* 2014).

Historical elevation profiles of extreme ESI illustrate the differences in vertical gradients between regions and demonstrate, such as for the NW, SW, and NE, notable departures from a steady linear drop-off with elevation (figure 3(a)). The moderating effect of water’s high specific heat, accentuated by coastal upwelling, is particularly apparent in the lower extreme ESI below 500 m in the NW, and to a lesser degree the SW. Across the US, extreme ESI drops off at a mean rate of around 4 °C per 1000 m, ranging from about a 4 °C difference over only 400 m in the MW to a 6 °C difference from 250 to 2250 m in the NW. This greater elevation dependence in the eastern

regions is correlated with their greater summertime RH (figure 3(a), scatterplot). Our hypothesis is that this follows from higher RH increasing the chance of precipitation; that precipitation removes moisture (the most important element for heat stress as per Raymond *et al* 2017); and this process is more and more likely to have occurred as one moves to higher elevations.

Looking more closely at patterns of extreme-ESI warming, we find approximately a 25% variation in the increase across regions at a given elevation, and about a 15% variation across elevations in a given region (figure 3(b)). A latitudinal gradient is apparent, with the northern US having larger increases especially below 750 m, driven by  $T$  (figure 2(a); Wuebbles *et al* 2015). This gradient may be a consequence of confounding between latitude and RH during extreme heat events, i.e. changes in extreme ESI are smaller where extreme ESI is more closely correlated with  $q$ —a relationship that broadly strengthens with latitude (Raymond *et al* 2017).

Echoing previous studies of both means and extremes, we find across regions sharply smaller increases at sea level than at higher elevations (figure 3(b)) (Rupp *et al* 2017, Zobel *et al* 2017). The eastern regions (MW, NE, SE) share a relatively small increase at the lowest elevations relative to 250 m (a coastal effect of about 0.25 °C), comparable to that found in Raymond and Mankin (2019)



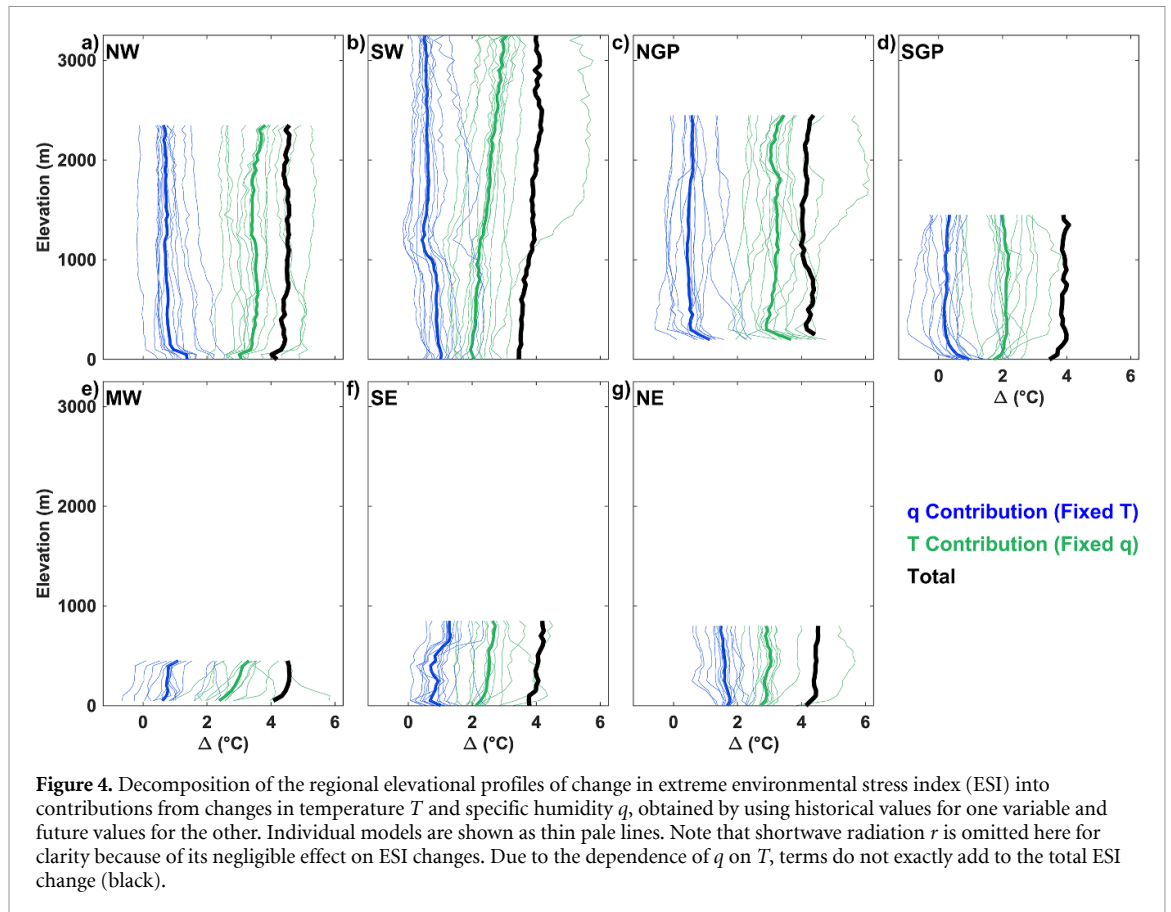


**Figure 4.** Decomposition of the regional elevational profiles of change in extreme environmental stress index (ESI) into contributions from changes in temperature  $T$  and specific humidity  $q$ , obtained by using historical values for one variable and future values for the other. Individual models are shown as thin pale lines. Note that shortwave radiation  $r$  is omitted here for clarity because of its negligible effect on ESI changes. Due to the dependence of  $q$  on  $T$ , terms do not exactly add to the total ESI change (black).

using datasets produced with different downscaling techniques (Pierce *et al* 2014, Zobel *et al* 2017). The SW and SGP are expected to see the least extreme-ESI increase, which is especially small at sea level, then rises about  $0.4\text{ }^{\circ}\text{C}$  from 0 to 1000 m, and in the SW a further  $0.4\text{ }^{\circ}\text{C}$  from 1000 to 2000 m (figure 3(b), red and gold lines) (Rangwala *et al* 2012). The SW's  $T$  and  $r$  increases are also the smallest of any region, possibly due to model projections of continuing or even strengthening marine-layer intrusions along the coast that offset any reductions in coastal cloudiness (Lebassi-Habtezion *et al* 2011). Above about 800 m, where the California marine-layer influence fades away, ESI changes in the SW are more similar to those in the NW and NGP (figure 3(b)). Models tend to underestimate the temperature difference between the interior and the coast on hot days by a factor of about 2 in the eastern US (Raymond and Mankin 2019), suggesting (if this model bias applies also in the western US) that the actual coastal increases may be even smaller than indicated here.

Spatially varying increases of extreme  $T$  and  $q$  contribute to shaping the elevational profiles of extreme ESI change (figure 4). Changes in extreme shortwave radiation exhibit almost no elevation dependence, so we exclude them from figure 4 for simplicity. For all regions and elevations, increases in  $T$  are the primary factor underlying increases in

ESI; however, in coastal areas below 250 m (i.e. for all regions except the NGP and MW),  $q$  increases have an ESI effect of similar magnitude (figures 2(c) and (f)). Extreme- $T$  increases have relatively greater importance at higher elevations, most notably in the West, and are nearly constant with elevation otherwise, except for a sharply smaller increase near sea level (figure 4). This apparent coastal effect is less noticeable in the SW than the NW; the latter has greater topographically induced localizing of cooling to the coast, even on extreme heat stress days (Rupp *et al* 2017). This phenomenon bears further examination in targeted studies. The greater  $q$  contribution at the lowest NGP elevations may be related to these being in the region's east and therefore substantially more humid than the central and western parts (figures 1(a) and S6(b)). In general,  $q$  contributions to ESI change tend to be largest near sea level and gradually smaller above 1000 m. However, because our method does not consider the dependence of  $q$  on  $T$ , it tends to underestimate (overestimate) the contribution of  $T$  ( $q$ ), particularly at higher elevations where there is a greater ratio of warming to moistening.

The high-resolution downscaled model output we employ retains biases in complex terrain and near large water bodies, such that higher-resolution regional modeling experiments might

yield significant upgrades in accuracy. Land-surface representations are well-known as potential sources of error, especially for extreme events (Cheruy *et al* 2014). Humidity and radiation are also broadly less reliable than temperature in both observations and simulations (Abatzoglou 2013). To identify patterns of extreme-heat-stress change, we have used only the RCP8.5 scenario due to its large warming signal; however, this limits our study's applicability to less severe scenarios, as there might be physical non-linearities that prevent our findings from being extrapolated. The choice of data resolution also shapes the results; considering ESI computed with daily-minimum temperature yields slightly different values and spatial patterns, with generally a greater increase in low-latitude coastal areas (figures S7 and S8). Framing our study using National Climate Assessment regions also means our conclusions may partly reflect uncorrected-for correlations across gridpoints within a region—for example, between elevation and latitude. We omit separate analysis of any urban effects the models may contain, because of their likely biases and because urbanized areas comprise only 1%–6% of the regional area fractions. But large urban areas considerably affect their local climate (as seen in both observational and model evidence) and tend to be located at low elevations within each region, so this omission may contribute to the non-linearities observed in figure 3(a), particularly in the more heavily urbanized Northeast.

Our results highlight several key attributes of projected extreme heat stress change in the US. The dominant feature is an increase of 3 °C–5 °C, leading to the late 20th-century top 1% summer heat stress occurring on about 25%–50% of summer days by the late 21st century. The majority of this relative increase is due to rising temperatures, although moisture increases are responsible for nearly half in the southern and eastern regions. Elevational variations in temperature and moisture changes add further detail to this picture. Compared to moderate-elevation areas, ocean coastlines experience smaller temperature increases not fully compensated by larger moisture increases. For example, along the Atlantic coast, nearly all models agree that extreme-ESI increases will be greater at 250 m than at sea level and at 500 m than at 250 m (figures 3(b) and S9). In the mountains of the West around 2000 m, extreme heat stress increases are greater than at 1000 m, but this differential increase is either small (approximately 0.3 °C) or statistically insignificant. Although heat stress intensity drops off with elevation, estimates of warming rate and the diagnosis of factors that might enhance it are crucial for accurately understanding risk—which is often connected more closely with relative extremes and rates of warming than with actual values—and for assessing the likelihood of unprecedented extreme events (Ward *et al* 2020, Fischer *et al* 2021).

## 4. Conclusions

Analysis of high-resolution statistically downscaled model projections indicates large increases in extreme heat stress across the US from the late 20th to the late 21st centuries under the RCP8.5 scenario, and that this increase is generally greater at higher latitudes and elevations. Our results aid in quantifying this broad picture and also newly reveal how heterogeneous spatial patterns of temperature and specific-humidity changes interact to shape it, including identifying hotspots of heat stress warming in the Sierra Nevada, central Rockies, and southern Appalachian Mountains. We find that in many regions large temperature increases cause extreme heat stress to rise at a somewhat faster rate at higher elevations, despite moisture increasing more at low elevations. As heat stress impacts are a function of both the rate of warming and the actual value, locations where one (or both) are especially large present a particular challenge for human health and for natural and managed systems. We find that the elevation dependence of observed heat stress exhibits regional differences that are correlated with coastal proximity and regional humidity, which bear an imprint on current and future values. Further observational and high-resolution modeling work would aid in determining how the regional patterns that we describe vary with local microclimates (especially urban-inflected ones) and specific events, while investigation of the human and landscape context in which intensified extreme heat stress events will occur is a necessary prerequisite for anticipating and mitigating their potential harm.

## Data availability statement

The data that support the findings of this study are openly available. The MACAv2-METDATA dataset can be accessed at [https://developers.google.com/earth-engine/datasets/catalog/IDAHO\\_EPSCOR\\_MACAv2\\_METDATA](https://developers.google.com/earth-engine/datasets/catalog/IDAHO_EPSCOR_MACAv2_METDATA). ERA5 reanalysis is available at [www.ecmwf.int/en/forecasts/datasets/reanalysis-datasets/era5](http://www.ecmwf.int/en/forecasts/datasets/reanalysis-datasets/era5), and HadISD is available at [www.metoffice.gov.uk/hadobs/hadis/](http://www.metoffice.gov.uk/hadobs/hadis/). Code necessary to reproduce the figures can be found at [www.github.com/cr2630git/raymondetal\\_heatstresselev](https://github.com/cr2630git/raymondetal_heatstresselev).

## Acknowledgments

A portion of this work was carried out at the Jet Propulsion Laboratory, California Institute of Technology, under a contract with the National Aeronautics and Space Administration (80NM0018D0004).

## Conflict of interest


The authors declare no conflicts of interest.

## ORCID iDs

Colin Raymond  <https://orcid.org/0000-0003-3093-5774>

Paul Loikith  <https://orcid.org/0000-0002-2352-0565>

Agniv Sengupta  <https://orcid.org/0000-0003-3687-5549>

Deepti Singh  <https://orcid.org/0000-0001-6568-435X>

## References

- Abatzoglou J T 2013 Development of gridded surface meteorological data for ecological applications and modelling *Int. J. Climatol.* **33** 121–31
- Abatzoglou J T and Brown T J 2012 A comparison of statistical downscaling methods suited for wildfire applications *Int. J. Climatol.* **32** 772–80
- Annear R L and Wells S A 2007 A comparison of five models for estimating clear-sky solar radiation *Water Resour. Res.* **43** 1–15
- Barnston A G, Lyon B, Coffel E D and Horton R M 2020 Daily autocorrelation and mean temperature/moisture rise as determining factors for future heatwave patterns in the United States *J. Appl. Meteorol. Climatol.* **59** 1735–54
- Broadbent A M, Krayenhoff E S and Georgescu M 2020 The motley drivers of heat and cold exposure in 21st century US cities *Proc. Natl Acad. Sci. USA* **117** 21108–17
- Brown E K, Wang J and Feng Y 2021 US wildfire potential: a historical view and future projection using high-resolution climate data *Environ. Res. Lett.* **16** 034060
- Chen X, Li N, Liu J, Zhang Z, Liu Y and Huang C 2020 Changes in global and regional characteristics of heat stress waves in the 21st century *Earth's Future* **8** e2020ef001636
- Cheng Y-T, Lung S-C-C and Hwang J-S 2019 New approach to identifying proper thresholds for a heat warning system using health risk increments *Env. Res.* **170** 282–92
- Cheruy F, Dufresne J L, Hourdin F and Ducharne A 2014 Role of clouds and land-atmosphere coupling in midlatitude continental summer warm biases and climate change amplification in CMIP5 simulations *Geophys. Res. Lett.* **41** 6493–500
- Coffel E, Horton R M and de Sherbinin A 2018 Temperature and humidity based projections of a rapid rise in global heat stress exposure during the 21st century *Environ. Res. Lett.* **13** 014001
- Collins M et al 2013 Long-term climate change: projections, commitments, and irreversibility *Climate Change 2013: The physical science basis. Contribution of Working Group I to the Fifth Assessment Report of the Intergovernmental Panel on Climate Change* ed T F Stocker et al
- Dosio A, Mentaschi L, Fischer E M and Wyser K 2018 Extreme heat waves under 1.5 °C and 2 °C global warming *Environ. Res. Lett.* **13** 054006
- Dunn R J H, Willet K M, Thorne P W, Woolley E V, Durre I, Dai A, Parker D E and Vose R S 2012 HadISD: a quality-controlled global synoptic report database for selected variables at long-term stations from 1973–2011 *Clim. Past* **8** 1649–79
- Dunne J P, Stouffer R J and John J G 2013 Reductions in labour capacity from heat stress under climate warming *Nat. Clim. Change* **3** 563–6
- Ferranti E, Chapman L, Lowe C, McCulloch S, Jaroszowski D and Quinn A 2016 Heat-related failures on Southeast England's railway network: insights and implications for heat risk management *Weather Clim. Soc.* **8** 177–91
- Fischer E M, Sippel S and Knutti R 2021 Increasing probability of record-shattering climate extremes *Nat. Clim. Change.* **11** 689–95
- Gao C, Kuklane K, Östergren P-O and Kjellstrom T 2017 Occupational heat stress assessment and protective strategies in the context of climate change *Int. J. Biometeorol.* **62** 359–71
- Guirguis K et al 2018 Heat, disparities, and health outcomes in San Diego County's diverse climate zones *GeoHealth*, **2** 212–23
- Hanna E G and Tait P W 2015 Limitations to thermoregulation and acclimatization challenge human adaptation to global warming *Int. J. Env. Res. Public Health* **12** 8034–74
- Haqiqi I, Grogan D S, Hertel T W and Schlenker W 2021 Quantifying the impacts of compound extremes on agriculture *Hydrol. Earth Syst. Sci.* **25** 551–64
- Harpold A A and Brooks P D 2018 Humidity determines snowpack ablation under a warming climate *Proc. Natl Acad. Sci.* **115** 1215–20
- Hersbach H et al 2020 The ERA5 global reanalysis *Q. J. R. Meteorol. Soc.* **146** 1999–2049
- Jiang Y, Kim J B, Still C J, Kerns B K, Kline J D and Cunningham P G 2018 Inter-comparison of multiple statistically downscaled climate datasets for the Pacific Northwest, USA *Sci. Data* **5** 180016
- Kjellstrom T, Briggs D, Freyberg C, Lemke B, Otto M and Hyatt O 2016 Heat, human performance, and occupational health: a key issue for the assessment of global climate change impacts *Annu. Rev. Public Health* **37** 97–112
- Knutti R, Masson D and Gettelman A 2013 Climate model genealogy: generation CMIP5 and how we got there *Geophys. Res. Lett.* **40** 1194–9
- Lebassi-Habtezion B, Gonzalez J and Bornstein R 2011 Modeled large-scale warming impacts on summer California coastal-cooling trends *J. Geophys. Res.* **116** D20114
- Li C, Zwiers F, Zhang X, Li G, Sun Y and Wehner M 2021 Changes in annual extremes of daily temperature and precipitation in CMIP6 models *J. Clim.* **34** 3441–60
- Li D, Yuan J and Kopp R E 2020 Escalating global exposure to compound heat-humidity extremes with warming *Environ. Res. Lett.* **15** 064003
- Lorenz R, Herger N, Sedláček J, Eyring V, Fischer E M and Knutti R 2018 Prospects and caveats of weighting climate models for summer maximum temperature projections over North America *J. Geophys. Res. Atmos.* **123** 4509–26
- Mankin J S, Smerdon J E, Cook B I, Williams A P and Seager R 2017 The curious case of projected twenty-first-century drying but greening in the American West *J. Clim.* **30** 8689–710
- Minder J R, Letcher T W and Liu C 2018 The character and causes of elevation-dependent warming in high-resolution simulations of rocky mountain climate change *J. Clim.* **31** 2093–113
- Mora C, Counsell C W W, Bielecki C R and Louis L V 2017 Twenty-seven ways a heat wave can kill you: deadly heat in the era of climate change *Circ. Cardiovasc. Qual. Outcomes* **10** e004233
- Moran D S, Pandolf K B, Shapiro Y, Heled Y, Shani Y, Mathew W T and Gonzalez R R 2001 An environmental stress index (ESI) as a substitute for the wet bulb globe temperature (WBGT) *J. Therm. Biol.* **26** 427–31
- Moran D S, Pandolf K B, Shapiro Y, Laor A, Heled Y and Gonzalez R R 2003 Evaluation of the environmental stress index for physiological variables *J. Therm. Biol.* **28** 43–49
- Palazzi E, Mortarini L, Terzago S and von Hardenberg J 2018 Elevation-dependent warming in global climate model simulations at high spatial resolution *Clim. Dyn.* **52** 2685–702
- Pascale S, Boos W R, Bordoni S, Delworth T L, Kapnick S B, Murakami H, Vecchi G A and Zhang W 2017 Weakening of the North American monsoon with global warming *Nat. Clim. Change* **7** 806–12
- Pepin N et al 2015 Elevation-dependent warming in mountain regions of the world *Nat. Clim. Change* **5** 424–30
- Pierce D W, Cayan D R and Thrasher B L 2014 Statistical downscaling using localized constructed analogs (LOCA) *J. Hydrometeorol.* **15** 2558–85

- Rangwala I, Barsugli J, Cozzetto K, Neff J and Prairie J 2012 Mid-21st century projections in temperature extremes in the southern colorado rocky mountains from regional climate models *Clim. Dyn.* **39** 1823–40
- Rangwala I, Sinsky S and Miller J R 2013 Amplified warming projections for high altitude regions of northern hemisphere mid-latitudes from CMIP5 models *Environ. Res. Lett.* **8** 024040
- Raymond C and Mankin J S 2019 Assessing present and future coastal moderation of extreme heat in the eastern United States *Environ. Res. Lett.* **14** 114002
- Raymond C, Singh D and Horton R M 2017 Spatiotemporal patterns and synoptics of extreme wet-bulb temperature in the contiguous United States *J. Geophys. Res. Atmos.* **122** 13,108–13,124
- Rupp D E, Li S, Mote P W, Shell K M, Massey N, Sparrow S N, Wallom D C H and Allen M R 2017 Seasonal spatial patterns of projected anthropogenic warming in complex terrain: a modeling study of the western US *Clim. Dyn.* **48** 2191–213
- Steadman R G 1979 The assessment of sultriness. Part II: effects of wind, extra radiation, and barometric pressure on apparent temperature *J. Appl. Meteorol.* **18** 874–85
- USGCRP 2017 *Climate Science Special Report: Fourth National Climate Assessment* vol I, ed D J Wuebbles *et al* (Washington, DC: U.S. Global Change Research Program) p 470
- Vicedo-Cabrera A M *et al* 2021 The burden of heat-related mortality attributable to recent human-induced climate change *Nat. Clim. Change.* **11** 492–500
- Vose R S, Easterling D R, Kunkel K E, LeGrande A N and Wehner M F 2017 *Temperature Changes in the United States* ed D J Wuebbles *et al* (Washington, DC: U.S. Global Change Research Program) pp 185–206
- Ward P J *et al* 2020 Natural hazard risk assessments at the global scale *Nat. Hazards Earth Syst. Sci.* **20** 1069–96
- Wu J, Zhou Y, Gao Y, Fu J S, Johnson B A, Huang C, Kim Y-M and Liu Y 2014 Estimation and uncertainty analysis of impacts of future heat waves on mortality in the eastern United States *Environ. Health Perspect.* **122** 10–16
- Wuebbles D *et al* 2015 CMIP5 climate model analyses: climate extremes in the United States *Bull. Amer. Meteorol. Soc.* **571**–83
- Zobel Z, Wang J, Wuebbles D J and Kotamarthi V R 2017 High-resolution dynamical downscaling ensemble projections of future extreme temperature distributions for the United States *Earth's Future* **5** 1234–51